POSITION AND ORIENTATION DEPENDENT ENERGY LANDSCAPES OF ANISOTROPIC COLLOIDAL PARTICLES IN NON-UNIFORM AC ELECTRIC FIELDS

by
Xiao Wang

A thesis submitted to Johns Hopkins University in conformity with the requirements for

the degree of Master of Science in Engineering

Baltimore, Maryland
May 2021

Abstract

Anisotropic colloidal particles are receiving more attention because of their potential applications in different aspects of scientific fields. It is important to reveal the principle driving the particle-field interaction to direct the manipulation and further introduce the assembly of anisotropic particles. Anisotropic particles made of photoresist material with different shapes and aspect ratios are fabricated using photolithography method, and the behavior of single particle in the non-uniform AC electric field is observed and recorded using optical microscopy. Boltzmann Inversion is applied to realize the quasi-2D analysis. From the generated position and orientation dependent energy landscapes, it is found that the ellipsoidal theory accurately models the behavior of elliptical prisms with only the particle conductivity as the adjustable parameter. To solve the discrepancy between elliptical theory and experimental result for the rectangular prisms with sharp rounded corners, other parameters related to the geometry of particle need to be introduced, and a great agreement between modified ellipsoidal model and experiment for rectangular prism can be found with the introduction of adjustable parameters along with physical restriction.

Advisor and primary reader: Michael A. Bevan

Secondary reader: Joelle Frechette

Acknowledgments

First, I would like to say thank you to Dr. Michael A. Bevan for giving me the precious opportunity to engage into the intriguing world of colloid science and teaching me the essential knowledge and experience to do the research and live my life. The motivation he gave me is really valuable, and I will treasure what I learned with a deep faith in the development and further application of colloidal science.

Second, I want to thank Dr. Joelle Frechette for giving me inspiration during her class and being the reader of my thesis. I would also like to thank all other faculties in the department and in the university for their crucial support during the hard time of pandemic.

Third, I really appreciate the help from my group. I would like to thank Rachel Stein for teaching me essential skills, giving me suggestions and having discussions with me during my program. I appreciate Lechuan Zhang for his help on doing better writing and presentation. I would also like to thank Dr. Dennis Neibloom for giving me help on designing a mask. I also appreciate Eugénie Jumai'an and Dr. Jianli Zhang for the discussions and helping me live a better life. I am grateful to Alex Yeh for giving advice on my project.

The support from my family is vital for completing my program, and I also want to say thank you to my friends who give me support during this program.

Table of Contents

List of Tables

List of Figures

1. Introduction

Controllable materials could significantly improve soft robotics,[1] active sensor[2] and advanced printing,[3] and thus their production and development is significant to both the scientific and industrial fields. One way to make it a reality is the promising ability of manipulating basic particles in micron-scale size as they can act as the building blocks of bulk materials.[4] As a key to realize many aspects of nano and micro technologies, the manipulation of colloidal particles is vital to be fully understood to direct the formation of high-tech materials. So far, many have studied the ways of controlling colloidal particles with external fields without direct contact[5]. As been reported by precedent work, optical tweezers,[6-10] magnetic field,[11-18] electric field,[19-22] and further developed plasmonic tweezers,[23] and optothermal manipulation based on the light induced temperature field[24] have been successfully utilized to manipulate the colloidal particles. Recently, some even combined the utilization of several tweezers to produce the mobile magnetic swimmers enabling the capability of trapping colloidal particles with optical field while controlling magnetic robots simultaneously,[25] which leaves a promising future on the polyphase manipulation of micron-scale matter.

Now, anisotropic particles are receiving much more attention because of their intriguing potential to bring into the field and industry of biomedicine[26] and assembly.[27] Precedent work has reported the realization of the fabrication of anisotropic particles[27-31] and thus having made the assembly of new anisotropic particles a reality. While applying external fields is one of the promising methods to take colloidal particles under control, the basic theory of manipulating anisotropic particles with external fields needs to be addressed as it is still uncertain as compared to the isotropic spherical particles. The requirement of rapid development in material and the demand from related fields demonstrate the urgent need of the understanding of principle driving

the manipulation of anisotropic particles. Thus, it is vital to further investigate the interaction of anisotropic particle when it is placed in external fields.

Many have focused on how the adjustment of external electric field determines the state of colloidal particle.[32] The dielectric particle is induced as dipole when being placed in electric field, but the equilibrium status is different when different kinds of electric fields are applied. DC electric field can trap the charged particle toward to edge that is oppositely charged.[33] By contrast, the AC electric field is versatile as the force it exert can be easily tuned by changing field parameters, and the particle can be at either the minima or maxima according to the condition of applied electric field.[34] The published works focusing on realizing the tunable colloidal assembly with rotating electric field[35] and controlling the assembly of Janus particles[36] also demonstrate the features of electric fields.

Precedent work has revealed some of the mysteries beneath the behavior of anisotropic particle under external field. Established theories are derived based on the polarization of spherical and ellipsoidal particles.[37] As has been proved by Rupp et al,[34] this ellipsoidal theory accurately modelled rod-like anisotropic particles with some adjustable parameters. However, the various shapes possessed by different anisotropic particles will further define the behavior of a particle in the field. Thus, although some has made some progress on understanding the particle-field interaction of rod-like particles, it is still necessary to study particles of other shapes to comprehend the difference brought by various geometries. Once single particle properties are better understood and the principle driving particle-field interaction is discovered, we can work towards applications of self-assembly that require several kinds of interactions. The particle-wall interaction, particle-particle interaction and particle-field interaction will combine as the net potential directing the self-assembly of colloidal particles. But, in order to simplify the complicated self-assembly

problem, it is essential to investigate each interaction separately to better understand the physical principles driving the behavior of anisotropic colloidal particles.

Herein, in our work, we successfully fabricated anisotropic particles in the shape of elliptical prisms and rectangular prisms. Developed using UV light, the particles are made of photoresist material SU-8 2002 and their patterns are directed by a pre-designed mask. We observed, recorded and studied the behavior of single anisotropic particles when they are placed under non-uniform AC electric fields. The particle-field interaction between induced dipole and electric field is investigated using the quasi-2D analysis involving the position and orientation dependent energy landscape of the newly prepared anisotropic particles. The particle conductivity is adjusted to meet the agreement between theory and experiment for elliptical prisms while the geometry factor related to the geometry of anisotropic particle is adjusted as the parameter for rectangular prisms to demonstrate the difference brought by the sharp rounded corners of rectangular prisms.

2. Theory

2.1 Anisotropic particle-field interaction

The three-dimensional anisotropic particle has six degrees of freedom, with three related to its position and three related to its orientation. The problem led by the different distribution of electric field set on different coordinates coordinate can be solved by setting lab and particle coordinate systems. The combined lab coordinate (x, y, z) system that aligns with the glass substrate, and particle coordinate (x', y', z') directions that align with the particle axes is set as the base for the general coordinate of three-dimensional anisotropic particle. The set angles (θ, φ, ψ) are defined for the orientation of anisotropic particle (Fig. 1a) with respect to the lab coordinates.

The general net potential of a single particle in electric field is given as

$$u^{net}\left(x,y,z,\theta,\phi,\psi\right)=u^{pw}+u^{pf}, \tag{1}$$

where u^{pf} is the particle-field interaction and u^{pw} is the particle-wall interaction.

Here, we investigate the particle-field interaction of anisotropic particles in the electric field along with the gravitational potential. For anisotropic particle, the gravitational potential is given as

$$u_g^{pf}=v_p\left(\rho_p-\rho_m\right)gz, \tag{2}$$

where v_p is the volume of particle, ρ_p is the density of particle, ρ_m is the density of medium, z is the distance between substrate wall and particle center, and g is the gravitational acceleration. The volume (v_p) for anisotropic particles changes with varying aspect ratio and geometry. For the tested particles, the volumes are given as

$$v_{p,e}=2\pi r_x r_y r_z, \tag{3}$$

$$v_{p,r}=8r_x r_y r_z, \tag{4}$$

where $v_{p,e}$ refers to the volume of elliptical prism, $v_{p,r}$ refers to the volume of rectangular prism, and r_x, r_y, r_z are the length of particle's semi-axes in each direction (Fig. 1b).

The general derived ellipsoidal particle-field interaction for a dielectric particle in a high frequency AC electric field is given as[37]

$$u^{pf}\left(x,\theta,y,z,\phi,\psi\right)=-\frac{3\varepsilon_m v_{p,j}}{4}\sum_{i=1}^{3}f_{CM,i}E_i^{'}\left(x,\theta,y,z,\phi,\psi\right)^2, \tag{5}$$

where E' electric field expressed in the particle coordinate system, and f_{CM} is the Clausius-Mossotti factor, defined along particle's each axis as[37]

$$f_{CM,i}=\mathrm{Re}\left[\frac{1}{3}\frac{\tilde{\varepsilon}_p-\tilde{\varepsilon}_m}{\tilde{\varepsilon}_m+\left(\tilde{\varepsilon}_p-\tilde{\varepsilon}_m\right)L_i^{'}}\right], \tag{6}$$

where L_i' is the shape-dependent depolarization factor, given as[38]

$$L_i^{'} = f_i L_i,$$
$$L_i = \frac{1}{2} r_x r_y r_z \int_0^\infty \frac{d\alpha}{\left(\alpha + r_i^2\right)\sqrt{\left(\alpha + r_x^2\right)\left(\alpha + r_y^2\right)\left(\alpha + r_z^2\right)}}, \tag{7}$$

where f_i is the defined adjustable multiplier for the shape-dependent depolarization factor, r_i is the corresponding semi-axis length of the particle. The initial values of f_i are 1 in all directions.

The complex permittivities are given as

$$\tilde{\varepsilon}_p = \varepsilon_p \varepsilon_0 - i\frac{\sigma_p}{\omega},$$
$$\tilde{\varepsilon}_m = \varepsilon_m \varepsilon_0 - i\frac{\sigma_m}{\omega}, \tag{8}$$

where ε is the permittivity, ε_0 is the free space permittivity, ω is frequency of electric field, and σ is the conductivity with the subscripts p and m referring to particle and medium respectively.

It should be noted that as an anisotropic particle is placed in solution, a surrounding electrostatic double layer will be formed above the particle surface. Thus, when the electric field is applied, the actual particle conductivity should be much higher than the material conductivity of SU-8 2002 due to polarization of the double layer ions.

2.2 Electric Field

The particle coordinate based electric field, ***E'***, needs to be transformed from ***E***, which is the electric field based on the lab coordinate using rotation transformation matrix A. ***E'*** is defined as

$$E^{'}\left(x,\theta,y,z,\phi,\psi\right) = A\left(\theta,\phi,\psi\right)\cdot E\left(x,y,z\right), \tag{9}$$

where the coordinate-based rotation transformation matrix A is given as

$$A(\theta,\phi,\psi) = \begin{pmatrix} \cos\theta\cos\psi - \cos\phi\sin\psi\sin\theta & \cos\theta\cos\psi + \cos\phi\cos\psi\sin\theta & \sin\theta\sin\phi \\ -\sin\theta\cos\psi - \cos\phi\sin\psi\cos\theta & -\sin\theta\sin\psi + \cos\phi\cos\psi\cos\theta & \cos\theta\sin\phi \\ \sin\phi\sin\psi & -\sin\phi\cos\psi & \cos\phi \end{pmatrix}, \quad (10)$$

The electric field $\boldsymbol{E}$ of a parallel coplanar electrode has two directions (Fig. 1d), given as[39]

$$\begin{aligned} \vec{E}(x,z) &= \left[E_x(x,z), E_z(x,z)\right], \\ E_x(x,z) &= \frac{2V_0}{\pi d}\left[\tan^{-1}\left(\frac{\sin\hat{x}}{\sinh\hat{z}}\right) - \tan^{-1}\left(\frac{\cos\hat{x}}{\sinh\hat{z}}\right)\right], \\ E_z(x,z) &= \frac{V_0}{\pi d}\left[\ln\left(\frac{\cosh\hat{z}+\cos\hat{x}}{\cosh\hat{z}-\cos\hat{x}}\frac{\cosh\hat{z}+\sin\hat{x}}{\cosh\hat{z}-\sin\hat{x}}\right)\right], \end{aligned} \quad (11)$$

where d is the electrode gap distance, V_0 is the voltage of electric field, and $\hat{x} = \pi(x+d)/2d + \pi/4$ and $\hat{z} = \pi z/2d$.

2.3 Quasi-2D analysis

As been reported by the precedent work,[34] the reduction of a six-dimensional (6D) energy landscape including 6 degrees of freedom to a two-dimensional (2D) energy landscape is required in order to be comparable to experiments where only position x and orientation θ can be observed. This is given by

$$\begin{aligned} p(x,\theta,y,z,\phi,\psi) &= \exp\left(-u^{pf}(x,\theta,y,z,\phi,\psi)\right), \\ \left\langle p(x,\theta)\right\rangle_{y,z,\phi,\psi} &= \frac{\int_{y_i}^{y_f}\int_{z_i}^{z_f}\int_{\phi_i}^{\phi_f}\int_{\psi_i}^{\psi_f} p(x,\theta,y,z,\phi,\psi)\,dydzd\phi d\psi}{(y_f-y_i)(z_f-z_i)(\phi_f-\phi_i)(\psi_f-\psi_i)}, \end{aligned} \quad (12)$$

where the transformation between probability and potential energy is obtained from Boltzmann Inversion. The reduced 2D probability can further be projected to a lower dimension and transformed to projected potential energy using Boltzmann Inversion as

$$\left\langle p(x)\right\rangle_{\theta} = \frac{\int_{\theta_i}^{\theta_f} \left\langle p(x,\theta)\right\rangle_{y,z,\phi,\psi} d\theta}{\left(\theta_f - \theta_i\right)}, \qquad \left\langle u(x)\right\rangle_{\theta} = -\log\left(\left\langle p(x)\right\rangle_{\theta}\right), \tag{13}$$

$$\left\langle p(\theta)\right\rangle_{x} = \frac{\int_{x_i}^{x_f} \left\langle p(x,\theta)\right\rangle_{y,z,\phi,\psi} dx}{\left(x_f - x_i\right)}, \qquad \left\langle u(\theta)\right\rangle_{x} = -\log\left(\left\langle p(\theta)\right\rangle_{x}\right), \tag{14}$$

It is feasible to generate one-dimensional (1D) position dependent and orientation dependent energy landscapes with separate comparison between theory and experiment.

It should be noted that although the anisotropic particles have six degrees of freedom, only five degrees of freedom are considered since the parallel electrode does not apply any field in the *y* direction, as seen in Eq. (11). The experiments, shown in Fig. 1(c) mean there is no *y* direction distribution for the electric field and the electric field only has distribution in *x* and *z* directions, as shown in Fig. 1(d).

2.4 Error minimization algorithm

The calculated error used in the process of acquiring the best fitted adjustable parameter is given as

$$Error = \sum\left(\left|u^{pf} - u^{\exp}\right|\right)^2, \tag{15}$$

where u^{exp} is the experimental potential energy. The found value of adjustable parameter with the minimal error is output as the best fitted result.

A weighted error (ξ) taking the error and the relative difference between the fitted value of f_i and the initial value of f_i into account is used to obtain the best fitted multiplier for the geometry factor, it is given as

$$r = \sqrt{\left(f_x - 1\right)^2 + \left(f_y - 1\right)^2 + \left(f_z - 1\right)^2},$$
$$\xi = Error \times \left(1 + r^2\right). \tag{16}$$

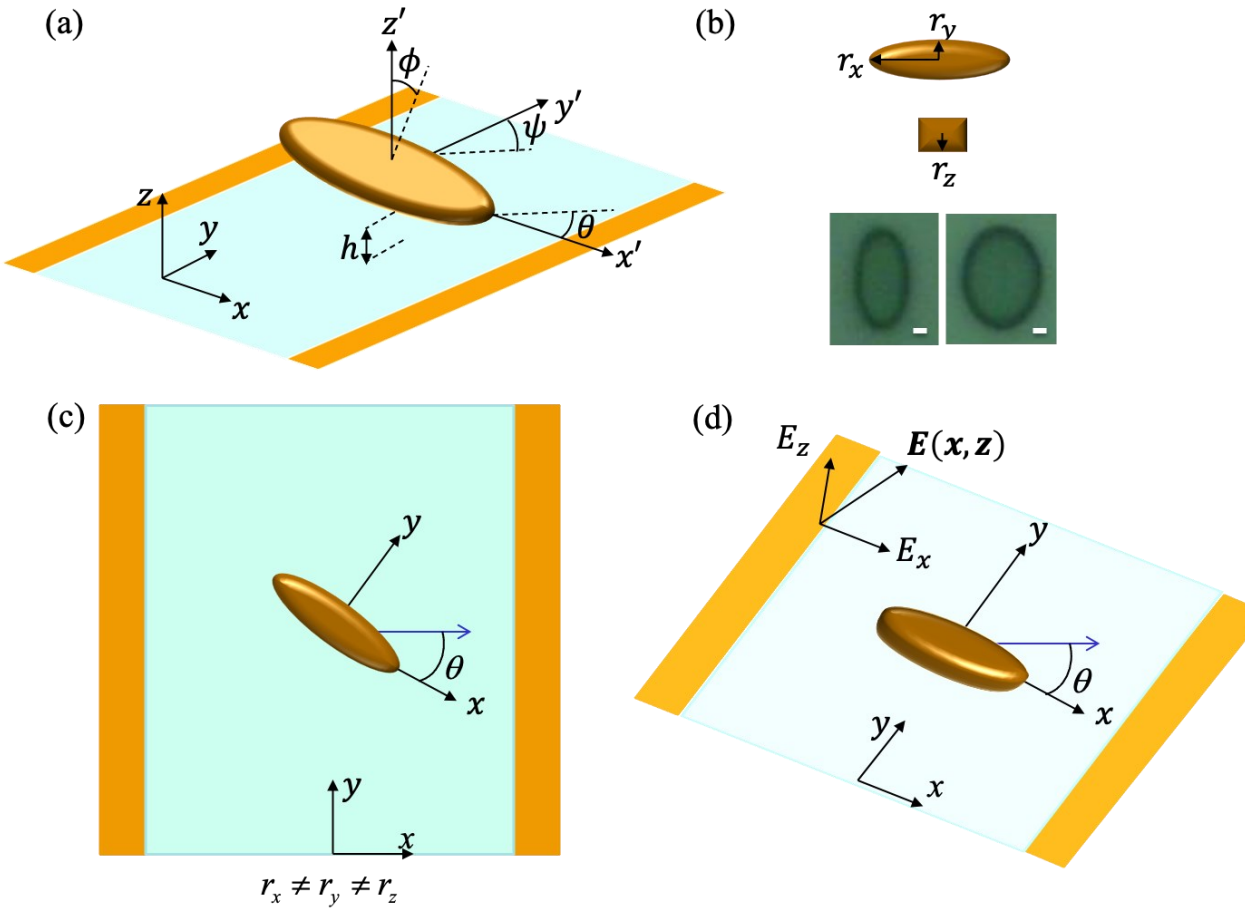

Figure 1. The schematic diagram of the elliptical prism and the electrode (a). The 3D diagram of elliptical prism with both the lab coordinate (x, y, z) system, and particle coordinate (x', y', z') along with the set orientation angles (θ, φ, ψ) (b). The dimensions (r_x, r_y, r_z) of elliptical prism and the image from optical microscopy with the 1-micron white scale bar (c). The quasi-2D analysis (x, θ) when a particle is placed in the electrode gap as viewed from above (d). The electric field generated by the coplanar parallel electrode including two directions (x, z)

3. Materials & Methods

3.1 Particle Fabrication

Anisotropic colloidal particles are fabricated using photolithographic method. Omnicoat (MicroChem) is first spin coated and cured on a silicon wafer as the base layer, then SU-8 2002 (MicroChem) is spin coated on the wafer as the material layer, which is then used to fabricate particles. Directed by a pre-designed photolithographic mask with a constant exposure energy for about 10 seconds, SU-8 2002 is cured by UV light with desired shapes sculpted. Developed by PG Developer (MicroChem) and rinsed using Isopropyl Alchohol, the SU-8 2002 material layer that have been cured by UV light is left on the wafer with residual SU-8 2002 washed off.

The SU-8 2002 material layer is charged by immersing in Sulfuric Acid for one minute. After rinsing off the residual Sulfuric Acid using DI water and being dried using pressured air, particles are released using PG Remover (MicroChem). The releasing process can be fastened by sonication. The PG Remover in solution is replaced by Isopropyl Alchohol during several times of centrifugation, and then Isopropyl Alchohol is replaced by DI water. Consequently, charged anisotropic particles are dispersed in DI water.

3.2 Experimental device

The gold patterned electrode is printed on a glass slide with specific geometry and a certain electrode gap (about 100 μm). The glass piece is sonicated in Acetone for 30 minutes, Isopropyl Alchohol for 30 minutes and placed still in Nochromix (Godax) for 25 minutes to clean the gold electrode. After cleansing, o-rings (McMaster-Carr) are attached to each edge of the electrode using high vacuum grease and copper wires are attached to the leads of the electrode. 30 mL of prepared solution with released particles is injected into the inner space created by o-rings and a cover slide is used to seal the experiment cell. The copper wires are connected to the Electricity Generator (Agilent 33220A) to insert AC signal.

3.2 Optical microscope and video analysis

Inverted Optical Microscopy (Zeiss) with a 63x objective along with CCD camera (Hamamatsu, Orca-ER) and Streampix (Norpix) are used to observe and record the position and orientation of particles. The recorded videos are 30 minutes long with 9000 frames at 5 fps. The position and orientation of particle are analyzed using a tracking program in MATLAB with the focus on using the brightness thresholding to tell the surrounding environment (dark) and the particle center with assigned length of semi-axes (bright).

4. Results & Discussion

4.1 Geometry and dimension of anisotropic colloidal particle

As been indicated by precedent work that the existing ellipsoidal theory works for rod-like particles,[34] elliptical prisms and elliptical prisms are successfully fabricated to further study the applicability of the ellipsoidal theory on particles with other shapes. The selected fabricated particles are shown in Fig. 2, with Fig. 2(a) - (c) showing the captured microscopy images for elliptical prisms with different aspect ratios using optical microscopy, and Fig. 2(d) - (f) shows the shapes of rectangular prisms with rounded sharp corners. The actual thickness varies for each particle, however, in order to eliminate the effect of z height in quasi-2D analysis, the thickness of all particles is fixed at an approximate value of 2 μm, as expected by the SU-8 material spin coating speed. As the patterns of selected particles are shown in Fig. 2, it can be stated that an ellipse is the most accurate top-view shape for (a-c), or elliptical prisms in 3D while (d-f) are the rectangles with slightly rounded corners, or as a rectangular prism in 3D. Thus, there should be some differences between the fabricated rectangular prisms and the true rectangular prisms, but it is reasonable to test these particles with some small flaw as this difference should have negligible effects on the corresponding results.

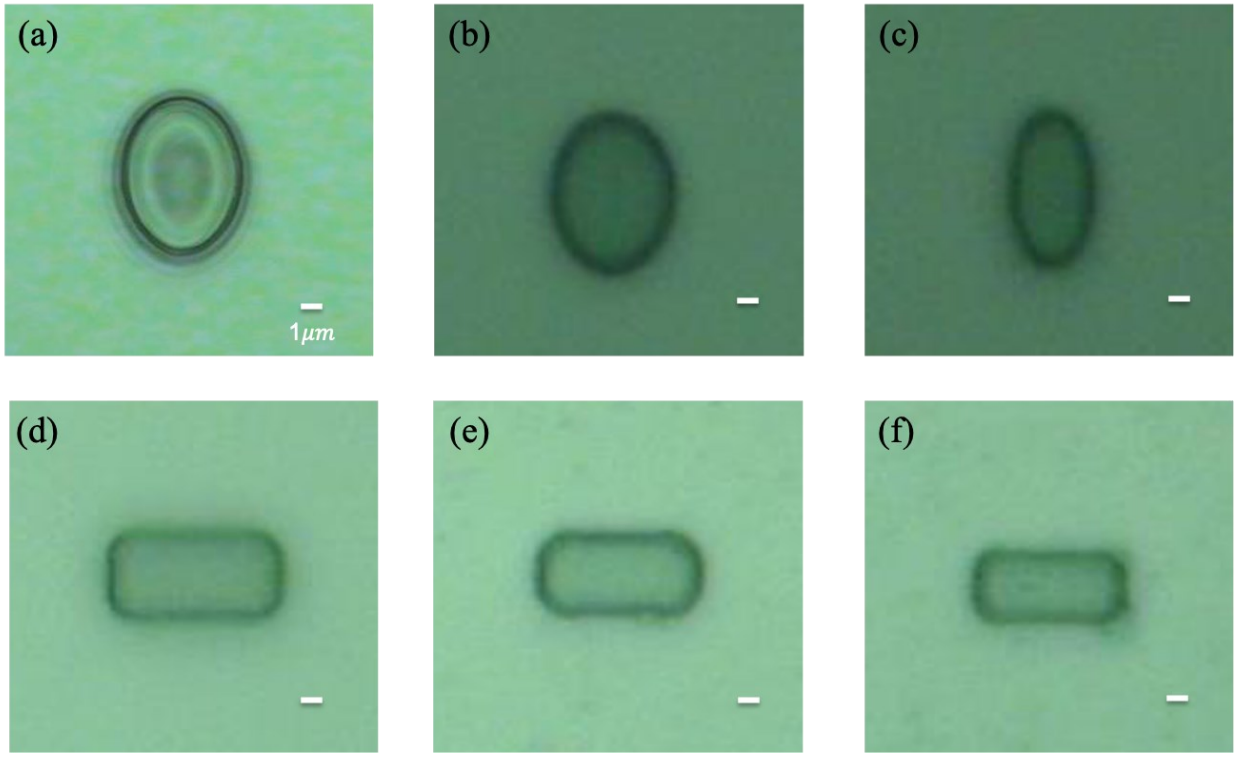

Figure 2. The geometry of anisotropic particles with different shapes and aspect ratios as viewed from above by optical microscopy (a). The elliptical prism with an aspect ratio of 1.28 (b). The elliptical prism with an aspect ratio of 1.30 (c). The elliptical prism with an aspect ratio of 1.75 (d). The rectangular prism with an aspect ratio of 2.11 (e). The rectangular prism with an aspect ratio of 2.12 (f). The rectangular prism with an aspect ratio of 2.29. All white scale bars are 1 micron.

Laser optical microscopy is used to measure the dimensions of our particles, which means it is supposed to have an uncertainty of about 0.3 μm in accordance with the wavelength of visible light. Thus, in order to reduce the bias that may be caused by the accuracy issue of visible light, we measured the inner (the smallest size according to the brightness of particle in Fig. 2) and outer (the biggest size) dimension of particles using scale bar. The measured scale bar pixel is used to calculate the particle dimension by making a comparison with the particle dimension pixels using ImageJ, and the mean dimension is taken as the definite dimension after having inner and outer sizes. The shape-dependent depolarization factor (L_i') can also be understood as a geometry factor, as seen in Eq. (6) and Eq. (7). The multipliers (f_i) for geometry factor are defined as 1 initially to observe the difference between the experimental results and existing ellipsoidal theoretical results.

4.2 Trajectory, probability and energy

The behavior of anisotropic SU-8 particles in non-uniform AC electric fields was measured by recording equilibrium motion of a single particle at a fixed frequency and voltage. Fig. 3 shows the analysis protocol of an experiment video recording. The trajectory of particle in the electrode gap is obtained from the recorded video to track the behavior of single particle. The particles in the recorded videos are captured and analyzed based on the brightness contrast they have against the environment, and the corrected absolute positions and orientations are saved as the experimental data.

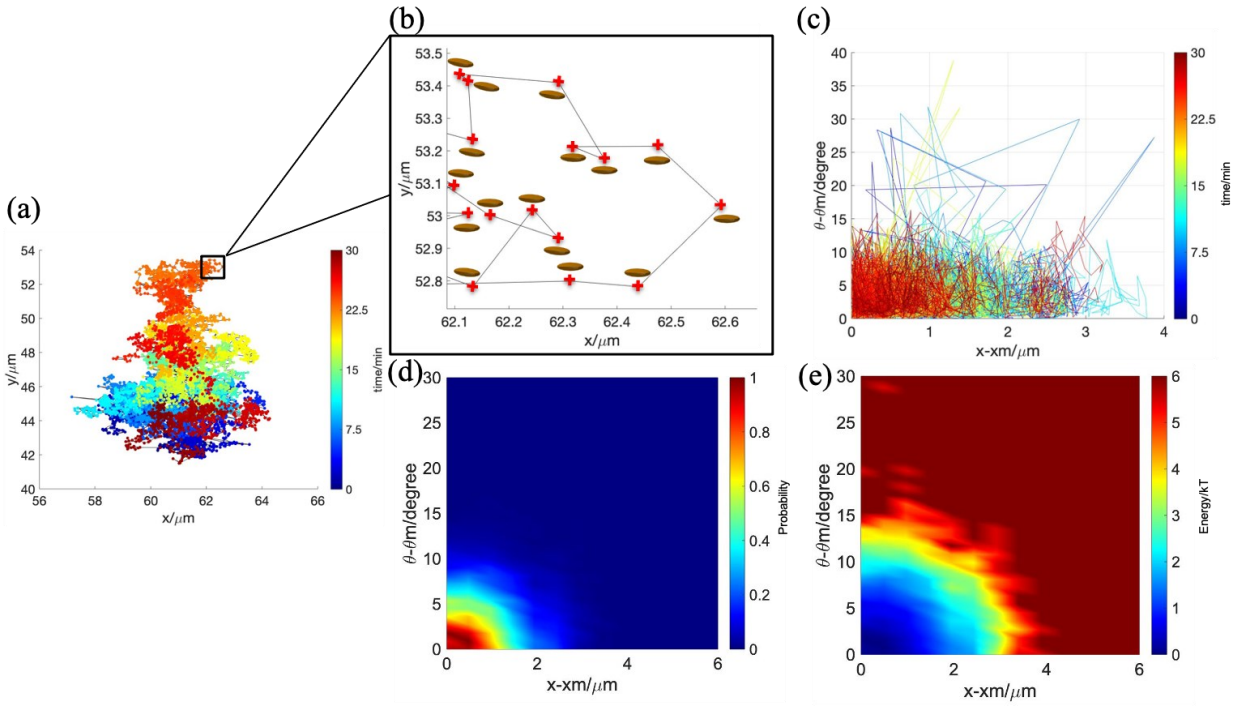

Figure 3. The conversion from trajectory of a particle sampling positions and orientations to a 2D energy landscape (a). The 2D trajectory from tracking video of a single particle with its x position and y position varying based on time (b). The zoomed in section with specific orientation schematics with a time interval of 0.2 seconds between two adjacent points (c). The 2D trajectory based on the particle's x position and orientation angle with the color bar representing time (d). The normalized relative probability (p) distribution based on the emergence frequency of each position and orientation, with values of p/max(p) (e). The 2D energy landscape converted from probability using Boltzmann Inversion using Eq. (12)

From tracked video recordings, the position detail (x, y) of a single particle center in non-uniform AC electric field is shown as Fig. 3(a) with the relative (x, y) position to the electrode gap

over a 30-minute 5fps recording under the electric field of 5MHz and 3V. Each point on the plot represents a single occurrence of a specific position and orientation with 9000 total points with an interval of 200 *ms* between each. The parallel electrode defines the distribution of applied electric field. Attached at the edges of the parallel electrode, the electric field only has a x and a z direction distribution, indicating that the particle is confined in x direction while free to move in y direction. The particle is also confined in z direction due to the gravitational force and substrate force (downward force) being greater than the electrical force (upward force). Fig. 3(b) shows a zoomed in section with additional information about particle orientation at each timepoint. Considering a recording interval of 200 *ms*, the particle would spend a total of 3 seconds sampling positions and orientations in this area. As what is talked in theory section, the movement of particle along y direction has no contribution on the redistribution of the formation of electrostatic double layer surrounding the particle because of the parallel electrode used in experiment. Consequently, the movement in y direction does not have an effect on the actual dipole-field interaction energy landscape, therefore the general theory in this work is actually five-dimensional (5D). It should be noted that we used quasi-2D analysis to study the dipole-field interaction of these anisotropic particles, which means what is observed and analyzed is the change of x position and θ orientation that is later converted to probability distribution, as shown in Fig. 3(c), combining the position and orientation status of single particle at over 30 minutes.

The probability of the emergence of the particle at a specific position can be calculated based on the frequency of a specific position generated from the trajectory in Fig. 3(a). The positions and orientations of particle are arranged due to their values, respectively, and histogram is formed based on the group the data is arranged according to the range of their values and the set bin value. The position (x) where the highest probability is found is taken as the relative zero

position for the calculation of relative probability. Similarly, the same protocol is applied to the analysis of the orientation (θ) with the relative zero orientation is taken where the maximum probability is found. The probability of the other positions and orientations based on the relative zero position and relative zero orientation showing the relative emerging probability is calculated based on the relative emergence frequency and shown as Fig. 3(d). Fig. 3(d) shows the normalized probability distribution of single particle, in which where the probability is closer to 1 means the particle is closer to the most probable state. From Fig. 3(c, d), what can be observed is that the most probable position and orientation are both 0, and excursions beyond $x = 3\ \mu m$ and $\theta = 15$ degrees are rarely seen, indicating the particle is trapped at such a specific state. As shown in Eq. (12), the projected energy potential can be calculated using the Boltzmann Inversion. It is clear that the potential energy will be lower if the corresponding probability is higher, thus, we can find the lowest energy at the relative zero position and relative zero orientation where the highest probability can always be found. By applying the Boltzmann Inversion, Fig. 3(e) is generated to show the details of the 2-dimensional energy landscape versus position and orientation. Energy potentials greater than 5 kT is neglected as the recorded videos cannot provide sufficient statistics to analyze the particle status with such low probability.

Table 1. Parameters used in the experiments to fit the theory to energy landscape and generate Fig. 3 to Fig. 6. Values obtained from: [a]manufacturer values (MicroChem), [b]handbook values,[40] [c]previous work,[41] [d]previous work,[42] [e]AC electric field generator read out, [f]optical microscopy.

parameter	value	parameter	value
$\varepsilon_p/\varepsilon_0$[a]	3.2	σ_m (μS/cm)[c]	12.6
$\varepsilon_m/\varepsilon_0$[b]	78	h (nm) [c, d]	150
ρ_p (kg/m^3)[a]	1200	f (MHz)[e]	5
ρ_m (kg/m^3)[b]	1000	Voltage (V)[e]	3
κ^{-1} (nm)[c]	30	d_g (μm)[f]	97

4.3 Fitting between ellipsoidal theory and experiments for elliptical prisms

Fig. 4 shows the analysis result for one tested elliptical prism using the protocol stated in Fig. 3 with the used constants shown in Table 1. The experimental result relating energy potential

and position (x) and orientation (θ) is shown as Fig. 4(a). In order to make the theory comparable to experiment, the reduction from 5D to 2D energy landscape needs to be processed. One feasible way is to use the integral to get rid of the effect of redundant parameters, which is called projection.[34] As shown in Eq. (12), to realize the projected theory, the 5D dipole-field interaction energy potential is generated and Boltzmann Inversion is used to transform the energy potential to probability, and the other three redundant parameters (z, ϕ, ψ) can be eliminated using integral. The 2D potential energy can be obtained using Boltzmann Inversion. The particle conductivity (σ_p) in Eq. (8) has been considered as an adjustable parameter to meet the agreement between experiment and theory in precedent work. Rupp et al. demonstrated their work on investigating the dipole-field interaction for superellipsoid anisotropic particles.[34] In their work, they made the conductivity of particle a variable depending on the geometry of each axis, keeping the conductivity in x and y axis the same while the conductivity in z axis different. However, as a material property, we believe the particle conductivity should be a constant. Thus, the conductivity of particle is again made an adjustable variable in this work, however, it is considered as a constant whichever axis it is for. In order to determine the particle conductivity with the best agreement between experiment and theory, an error minimization algorithm (Eq. (15)) in MATLAB was used to find the minimal difference between theoretical result and experimental result when inserting different values. After the conductivity value with a minimal error is found, the value is inserted back in the theory to observe the actual gap between theory and experiment. As shown in Fig. 4(b), the theoretical result is a 2D energy landscape with (x, θ) based on the quasi-2D analysis using projected theory with the found best fitted conductivity. The 2D energy landscape shows the energy potential versus position and orientation for the tested particle, and when the color gets red, the corresponding energy is higher, closer to 5 kT, and the corresponding energy is lower when the

color gets blue, closer to 0 kT. By making a comparison between the experimental energy landscape (Fig. 4a) and theoretical energy landscape (Fig. 4b), the difference between them can be observed more clearly as shown in Fig. 4(c). In Fig. 4(c), the difference is closer to 0 kT when the color is green, and the difference is getting bigger when the color is orange or red. As shown by Fig. 4(c), the difference between theory and experiment is slight with excellent agreement, thus proving the ellipsoidal theory has a good fitting agreement with the experimental result.

To demonstrate the validity of ellipsoidal theory for elliptical prism more clearly, 1D energy landscapes are also generated as Fig. 4(d). The 2D energy landscape is separated into two individual 1D energy landscape using Eq. (13) and Eq. (14), the gap between points (experimental data) and lines (theoretical data) can be more clearly observed from Fig. 4(d), where blue is for the position dependent energy landscape and red is for the orientation dependent energy landscape. From the plotted lines and generated points, we can state that the theoretical lines have excellent agreement with experimental points, and thus demonstrating that the ellipsoidal theory is working well for elliptical prisms with no needed modifications.

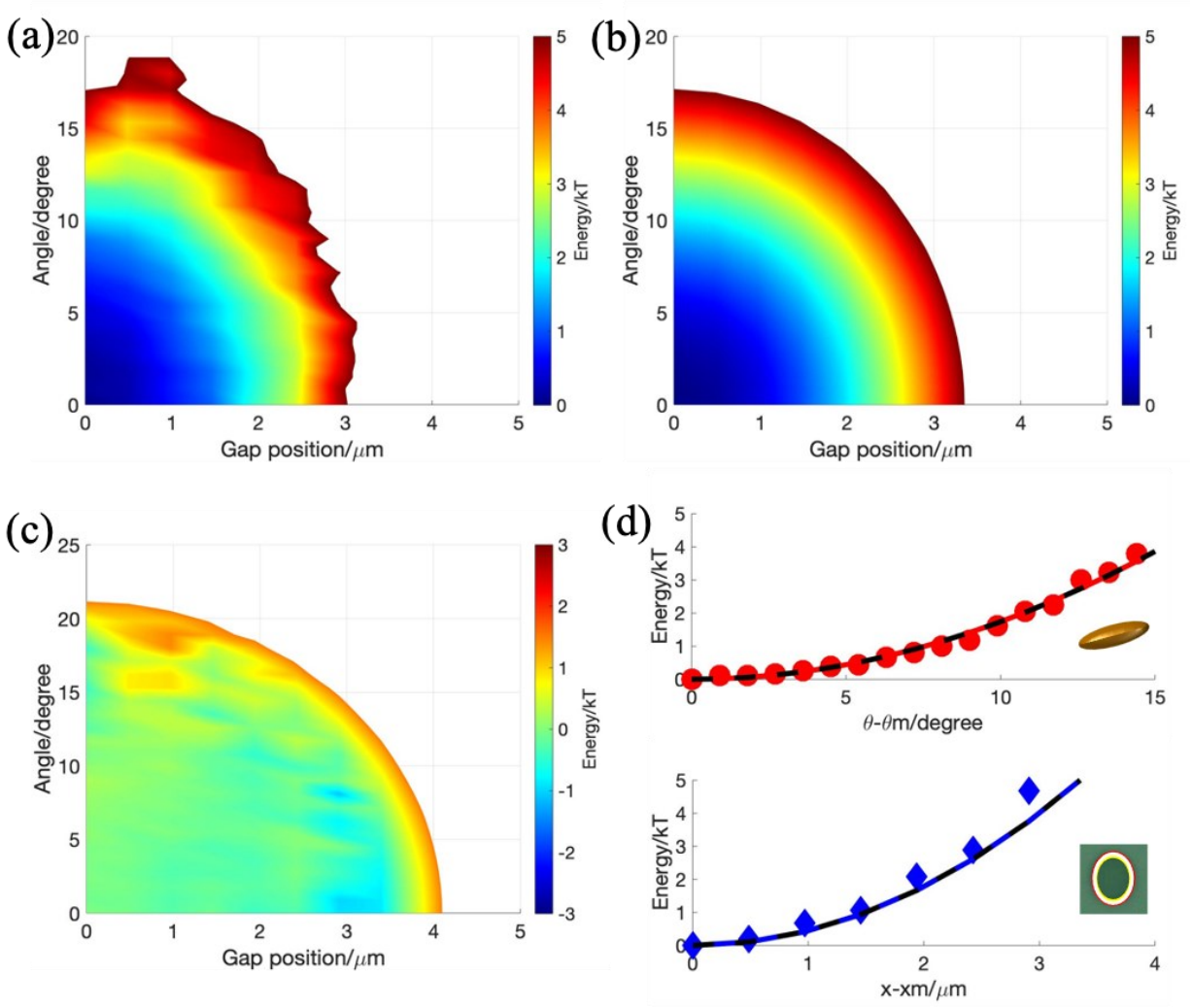

Figure 4. The fitting result of the theoretical ellipsoidal model to statistics from an elliptical prism with an aspect ratio of 1.15 (a). The experimental energy landscape generated from position and orientation statistics from a tracking video (b). The theoretical energy landscape of an ellipsoid of equivalent aspect ratio using Eq. (2) - (12) (c). The difference between 2D experimental and theoretical results (d). The projected and sliced1D energy landscape using Eq. (13) - (14), where red line and points are for orientation dependent energy landscape, blue line and points are for position dependent energy landscape, and black dash lines are for position and orientation dependent sliced theory

Besides projection, another possible way to do the reduction is using most probable (slice) theory to directly calculate the 2D dipole-field interaction with the redundant parameters fixed at the most probable value. The heavy dielectric plastic anisotropic particle staying at a fixed height and orientation relative to the electrode provides the possibility of applying slice theory on our model. In our model, based on the coordinate set for anisotropic particle as shown in Fig. 1(a), the most probable status of a particle when the electric field is applied is parallel to the electric field,

which means the long axis of the particles should be perpendicular to the edge of the electrode gap. In this status, the angles (ϕ, ψ) should be both 0. The specific z height, which is also known as the particle center elevation, is considered to be 5 times the length of Debye length based on precedent work,[42] and this gives the most probable height (h) equivalent to 1.5 r_z. The 1D sliced theoretical results are shown as black dash lines in Fig. 4(d), indicating that both ways accurately model the experiment.

Table 2. Particle dimensions and obtained conductivity values from fitting between ellipsoidal theory and experiment of elliptical prisms. Particle conductivity (σ_p) in the table is the fitted value to make the ellipsoidal theory match the 2D experimental energy landscape for elliptical prisms. Values obtained from: [a]optical microscopy

Particle	r_x, r_y, r_z (μm)[a]	Aspect Ratio	σ_p (μS/cm)	Multiplier (f_x, f_y, f_z)
1	3.9, 3.4, 1	1.15	108	1, 1, 1
2	3.7, 2.9, 1	1.28	114	1, 1, 1
3	3.5, 2.7, 1	1.30	111	1, 1, 1
4	3.5, 2.0, 1	1.75	114	1, 1, 1

Apart from the result shown in Fig. 4, other elliptical prisms are tested to fulfil the validity of applying ellipsoidal theory on elliptical prisms. As shown in Fig. 5, when the same protocol is applied for other elliptical prisms with different aspect ratios, a good fitting agreement between theory and experiment can always be found in both 2D and 1D energy landscapes. As shown in Fig. 2, the change of aspect ratio results in an obvious differentiation of geometry, so that the particle-field interaction is meant to be changed as many related parameters, including the dimension, volume and geometry factor are going to change corresponding to the geometric diversity as shown in Eq. (2) - (7). The results shown in Fig. 4 and Fig. 5 for the tested elliptical prisms with different aspect ratios along with the discovered conductivity values of 108, 114, 111 and 114 for each particle indicates each tested particle has a quite small discrepancy between theory and experiment with relatively similar conductivity values. The results from figures and Table 2 verify the applicability of ellipsoidal theory on elliptical prism. This result again supports the hypothesis that the conductivity, as a material property, should be consistent and independent

of axis length. The results of conductivity are quite similar, and if the average of these results is taken as the general conductivity value for SU-8 2002 in DI water, an approximate value of 110 can be taken as the general conductivity value and be used in further investigation.

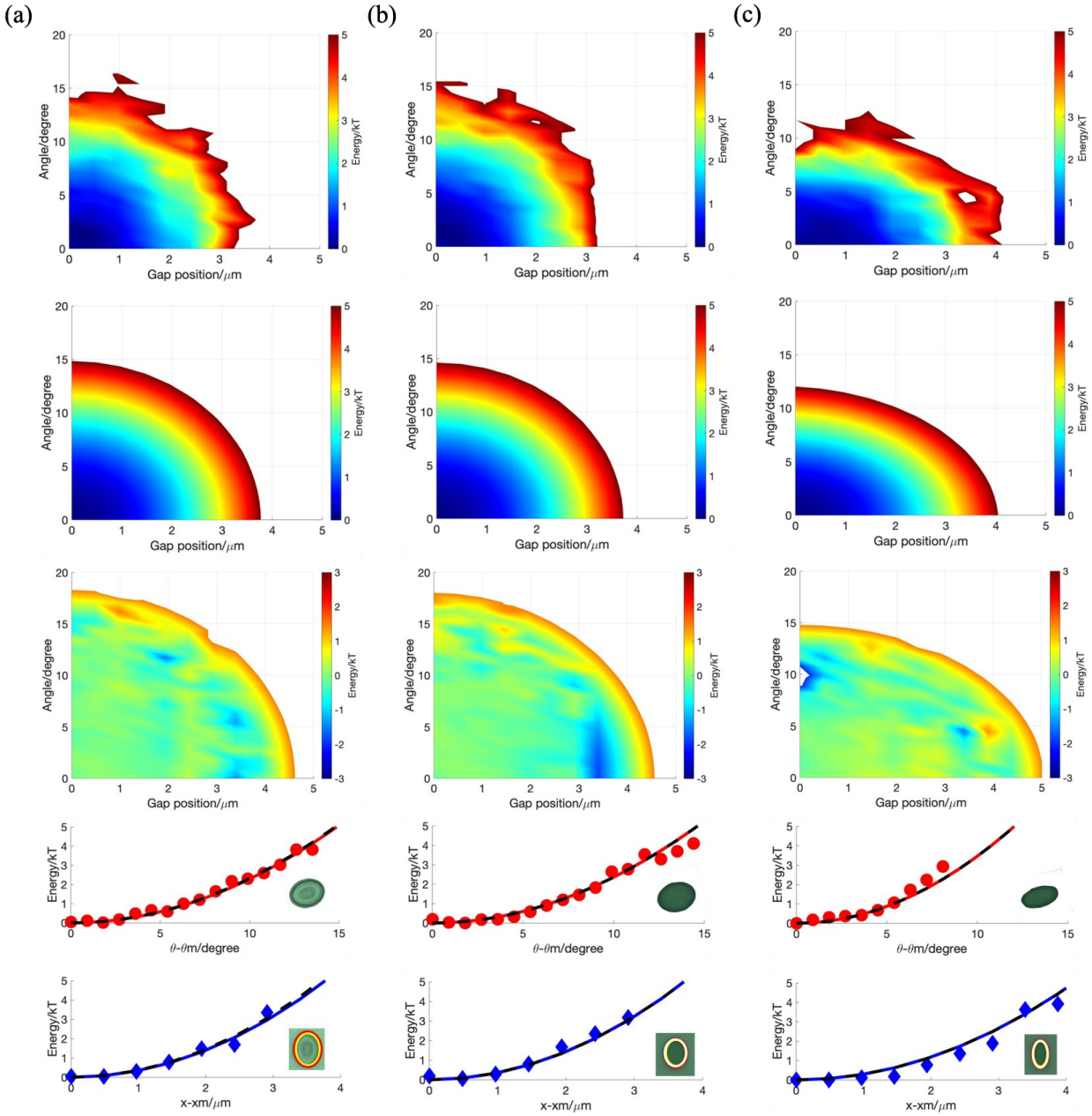

Figure 5. The fitting result of the theoretical ellipsoidal model to statistics from elliptical prisms with various aspect ratios. The first row is the experimental energy landscapes generated from (x, θ) statistics from particle tracking videos. The second row is for the theoretical energy landscape of an ellipsoid with an equivalent aspect ratio using Eq. (2) - (12). The third row shows figures showing differences between 2D experimental and theoretical results. The fourth row shows the 1D orientation dependent energy landscapes with red points for experimental results, red solid lines for projected theory and black dash lines for slice theory. The fifth row shows the 1D position dependent energy landscapes where blue points are for experimental results, red solid lines are for projected theory and black dash lines are for slice theory (a). The fitting result for the elliptical prism with an aspect ratio of 1.28 (b). The fitting result for the elliptical prism with an aspect ratio of 1.30 (c). The fitting result for the elliptical prism with an aspect ratio of 1.75

4.4 Fitting between ellipsoidal model and experiment for rectangular prism

In Fig. 6, the same method is applied to a rectangular prism with an aspect ratio of 2.11 at the same voltage and frequency of 3V and 5MHz. The analysis process of experimental data uses the same procedure of calculating histogram and Boltzmann Inversion to first generate the probability and then generate the 2D energy landscape of the tested rectangular prism as the quasi-2D analysis is used for rectangular prisms. The volume of rectangular prism (Eq. (4)) is used in the analysis process. The experimental energy landscape is shown in Fig. 6(a) and the theoretical energy landscape is shown in Fig. 6(b). For the theoretical model, as a general conductivity value for SU-8 2002 in DI water has been obtained, the conductivity of 110 is thus applied for the analysis of rectangular prisms. However, it is shown in Fig. 6(c, d) that there is large discrepancy between experimental points and theoretical lines if the ellipsoidal theory is applied. This means the existing ellipsoidal theory does not model the behavior of rectangular prisms with sharp rounded corners.

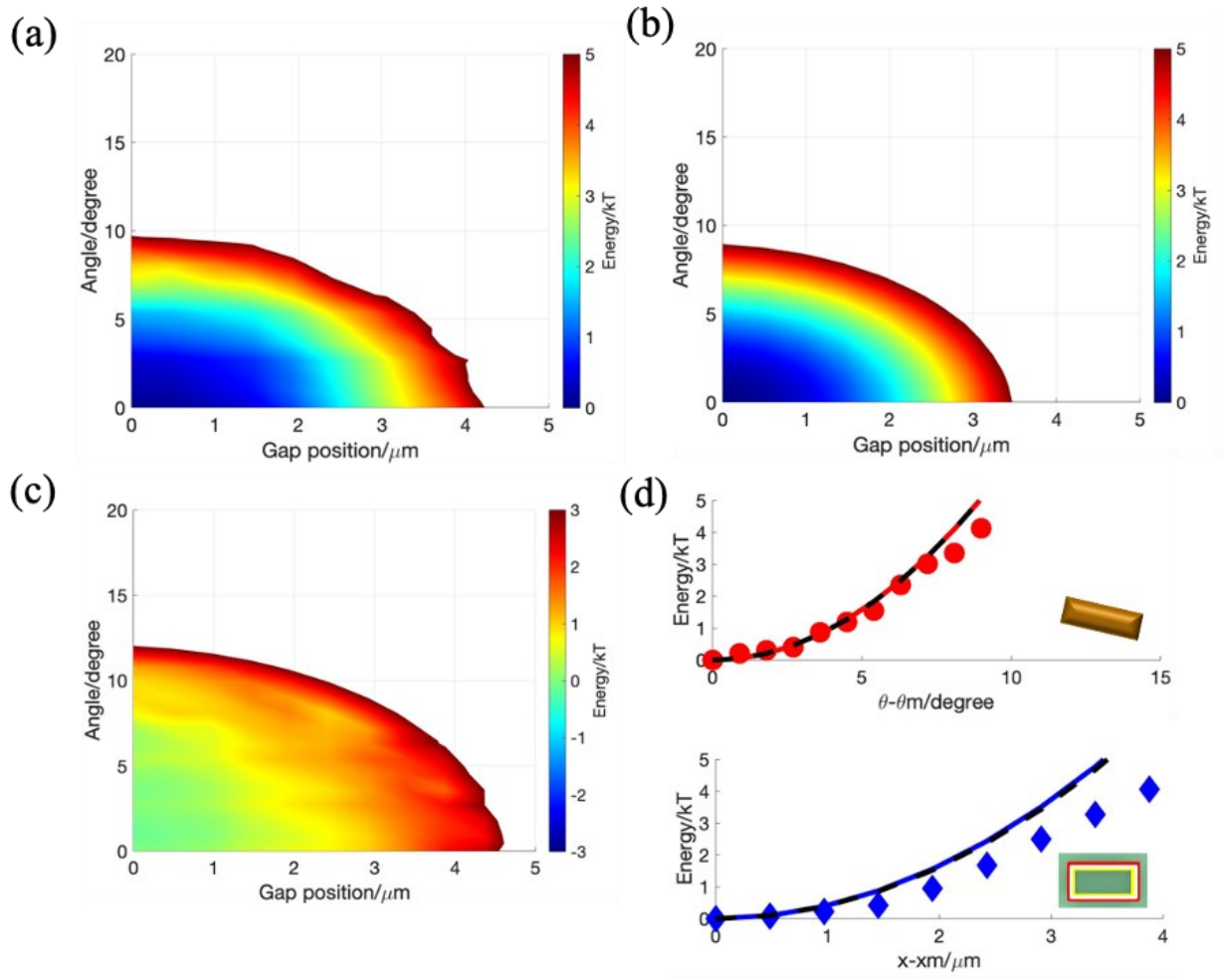

Figure 6. The fitting result of the ellipsoidal model to position and orientation statistics of a rectangular prism with an aspect ratio of 2.11. (a). The experimental energy landscape generated from (x, θ) statistics from tracking video (b). The theoretical energy landscape of an ellipsoid of equivalent aspect ratio using Eq. (2) - (12) (c). The difference between experimental and theoretical results (d). The projected and sliced1D energy landscape using Eq. (13) - (14), where red line and points are for orientation dependent energy landscape, blue line and points are for position dependent energy landscape, and black dash lines are for position and orientation dependent sliced theory

Thus, instead, inspired by the difference between elliptical prisms and rectangular prisms, some parameters are introduced to solve the noncompliance issue as the multiplier (f_i) for geometry factor (L_i') as shown in Eq. (7). The multiplier (f_i) is introduced as the essential difference of elliptical prism and rectangular prism is the geometric diversity taking the sharp corners of rectangle into account. As a three-dimensional particle, we introduced the multiplier for geometry factor in every direction of the coordinate (f_x, f_y, f_z) to be adjustable to solve the noncompliance

problem. The initial values of (f_x, f_y, f_z) are all 1, and various values of (f_x, f_y, f_z) in the range of 0 to 2 are inserted in the error minimization algorithm to help adjust the geometry factor (L_i') corresponding to the depolarization difference led by the specific geometry of rectangle. Fig. 7 shows the results of adjusting the multiplier for the same rectangular prism in Fig. 6. The experimental energy landscape is shown as Fig. 7(a). From Fig. 7(b), it is clear that a combination of 0.28, 0.54, 1.2 for (f_x, f_y, f_z) can be found with the minimal error that results in excellent agreement between theory and experiment. However, as we dug deeper into the intrinsic meaning of f_i in order to explain the difference it brought about, it is found that several combinations of f_i can be found with a quite small error. They are also acceptable as the systematic error in experimental points can hardly be completely removed thus leaving a possibility that multiple combinations can be accepted since we have to tell the stand or fall of these results by observing the difference visually. As shown in Fig. 7(c), a combination of 1, 0.95, 1.2 for (f_x, f_y, f_z) only adjusting f_y and f_z while keeping f_x constant at 1 is working for the fitting program. Therefore, based on what has been discovered so far, a general conclusion of the meaning of f_i is not achievable and some physical restrictions are needed to constrain the adjustment of f_i and thus obtain the physical principles for rectangular prisms.

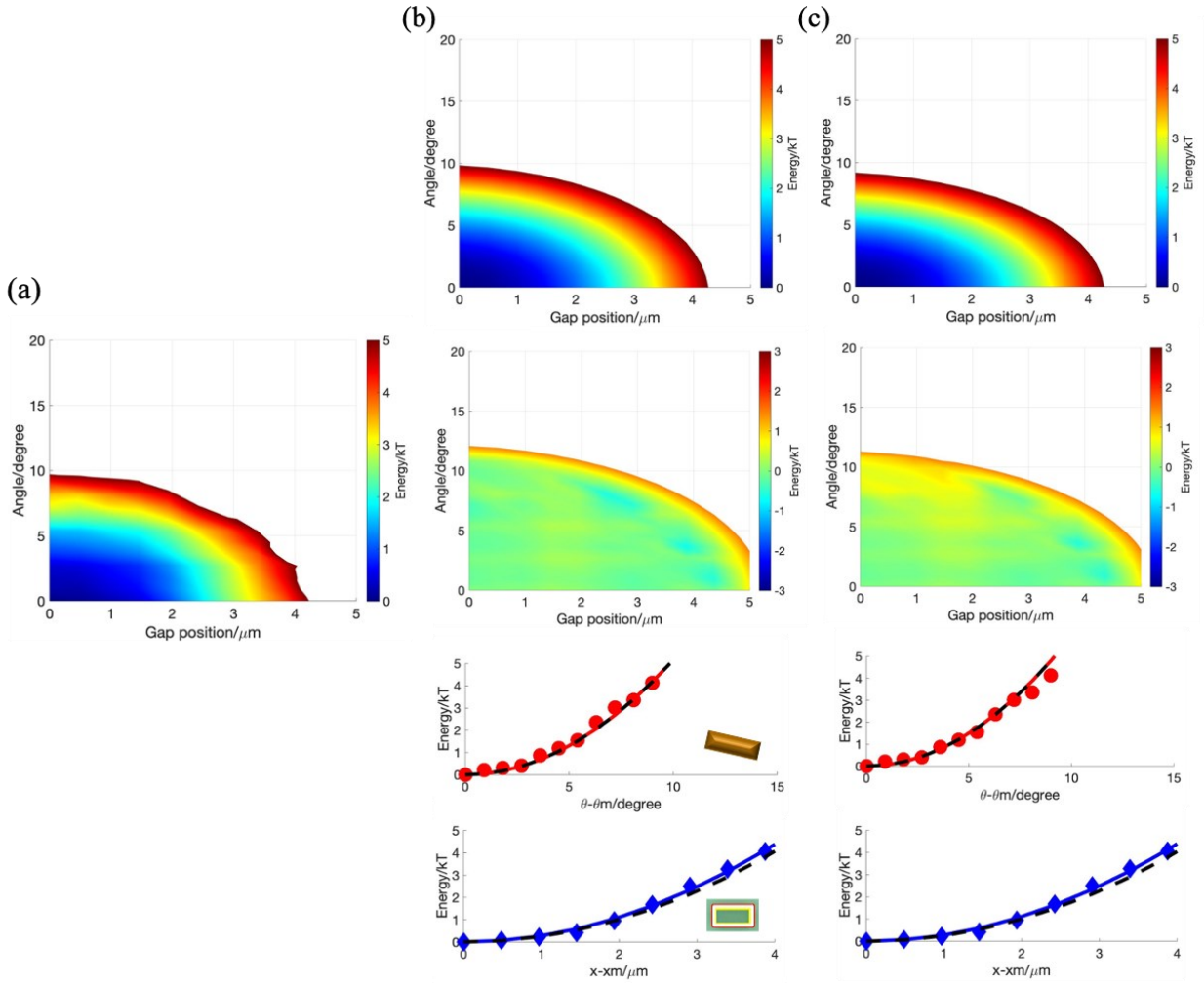

Figure 7. The fitting result of the modified ellipsoidal model to position and orientation statistics of a rectangular prism with an aspect ratio of 2.11 with the multiplier for geometry factor as the adjustable parameter. The first row shows the theoretical energy landscape of an ellipsoid with an equivalent aspect ratio using Eq. (2) - (12). The second row shows the differences between 2D experimental and theoretical results. The third row shows the 1D orientation dependent energy landscapes with red points for experimental results, red solid lines for projected theory and black dash lines for slice theory. The fourth row shows the 1D position dependent energy landscapes where blue points are for experimental results, red solid lines are for projected theory and black dash lines are for slice theory (a). The experimental energy landscape generated from (x, θ) statistics from tracking video (b). The fitting result between experiment and modified ellipsoidal theory with multipliers (f_x, f_y, f_z) of (0.28, 0.54, 1.2) (c). The fitting result with multipliers (f_x, f_y, f_z) of (1, 0.95, 1.2).

To solve the fluctuating result of adjusting the multiplier for geometry factor, we applied the physical principle that adding up geometry factor (L_i') in all directions should be equal to 1, which was indicated in precedent work.[43-44] A weighted error, shown in Eq. (16), is used to consider the difference between theory and experiment and the relative difference from the initial

value of f_i simultaneously. The fitting result is shown as Fig. 8. As shown in Fig. 8(a), the result of fitting modified ellipsoidal theory to experiment for a rectangular prism with an aspect ratio of 2.11 with the multiplier as the adjustable parameter indicates that a result of 0.75, 0.73, 1.19 for (f_x, f_y, f_z) works well to fulfill the applied restriction. And it gives the trend that (f_x, f_y) are smaller than 1 while f_z is bigger than 1. Fig. 8(b) also shows the same trend for another rectangular prism with an aspect ratio of 2.12 with a result of 0.88, 0.67, 1.21 for (f_x, f_y, f_z), which is shown in Table 3. This result shows that introducing multiplier for geometry factor as the adjustable parameter to modify the existing ellipsoidal theory is working for rectangular prisms with similar fitting outcome for different particles.

Table 3. Particle dimension and obtained multiplier values from fitting between theory and experiment of rectangular prisms. f_x, f_y, f_z in the table are the fitted values of multipliers to make the theoretical ellipsoidal model to match the 2D experimental energy landscape for rectangular prism. Values obtained from: [a]optical microscopy

Particle	r_x, r_y, r_z (μm)[a]	Aspect Ratio	σ_p (μS/cm)	Multiplier (f_x, f_y, f_z)
1	3.8, 1.8, 1	2.11	110	0.28, 0.54, 1.2
				1, 0.95, 1.2
				0.75, 0.73, 1.19
2	3.6, 1.7, 1	2.12	110	0.88, 0.67, 1.21

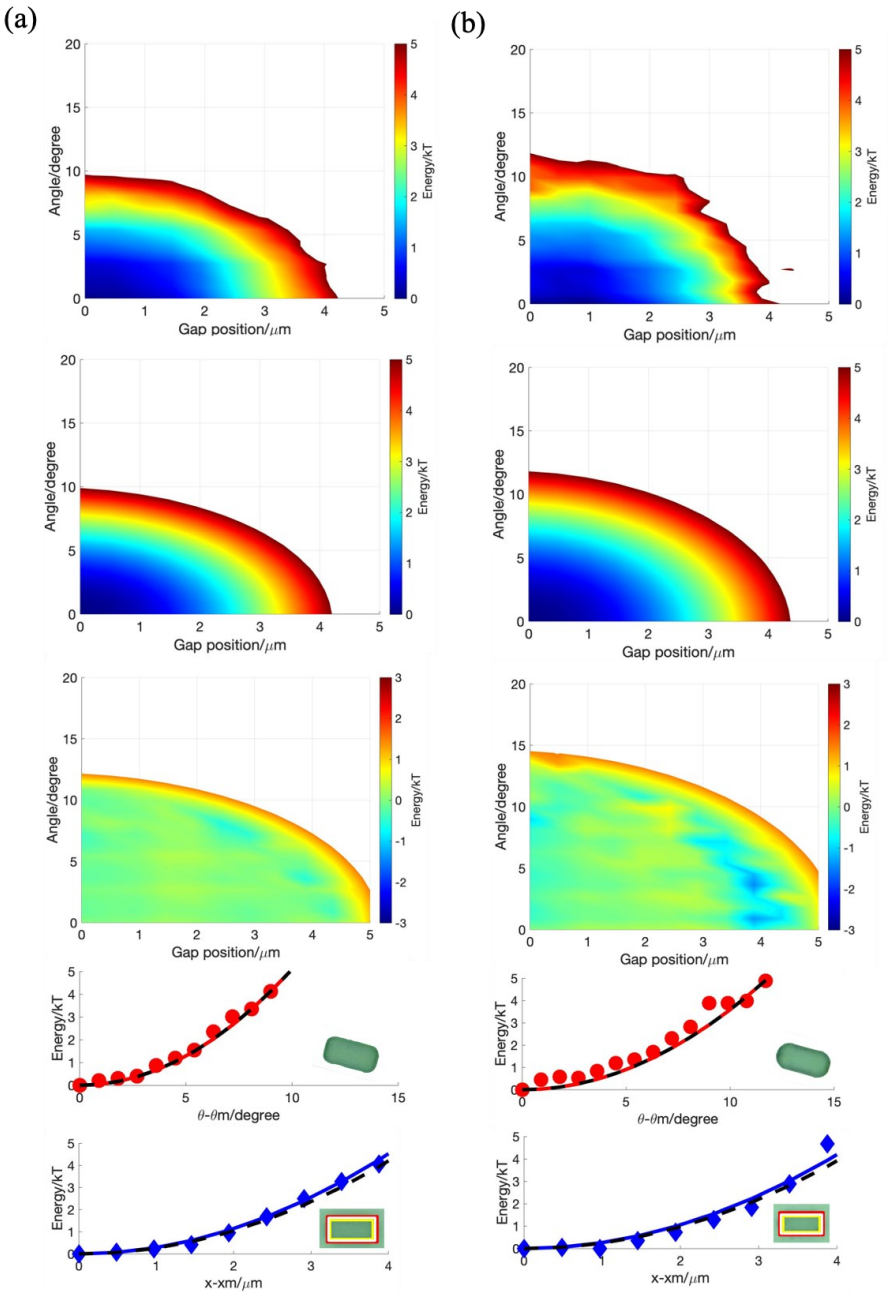

Figure 8. The fitting results of the modified ellipsoidal model to position and orientation statistics of rectangular prisms with different aspect ratios with the multiplier for geometry factor as the adjustable parameter and physical restriction applied. The first row shows the experimental energy landscapes generated from (x, θ) statistics from particle tracking videos**.** The second row shows the theoretical energy landscape of an ellipsoid with an equivalent aspect ratio using Eq. (2) - (12). The third row shows the differences between experimental and theoretical results. The fourth row shows the 1D orientation dependent energy landscapes with red points for experimental results, red solid lines for projected theory and black dash lines for slice theory. The fifth row shows the 1D position dependent energy landscapes where blue points are for experimental results, red solid lines are for projected theory and black dash lines are for slice theory (a). The fitting result between experiment and modified ellipsoidal theory with multipliers (f_x, f_y, f_z) of (0.75, 0.73, 1.19) for the particle with aspect ratio of 2.11 (c). The fitting result with multipliers (f_x, f_y, f_z) of (0.88, 0.67, 1.21) for the particle with aspect ratio of 2.12.

In the previous discussion, we have proven that both the projection and slice work for the fitting between theory and experiment. They should have a quite similar result since they are all based on the quasi-2D analysis, but sometimes we can still notice a slight difference between projection and slice because of the specific value of redundant parameters, as shown in the fifth row in Fig. 8(a, b). For the sliced theory, we need three specific values for (z, ϕ, ψ) respectively. But in the degradation process of projection, the discovered most probable height may be slightly deflected because of the geometric difference rectangular prism brings about. However, the slight discrepancy between projection and slice is still acceptable. This demonstrates that the simpler calculations at the most probably height z, and rotations ϕ, ψ can still accurately model particle-field behavior with less computational complexity. Therefore, further research in quasi-2D can use a simplified model while systems with higher degrees of freedom can still be modelled using five degrees of freedom. Thus, a simpler model can be applied on further research on investigating the meaning of f_i for rectangular prisms and it will help us find out the principle driving the interaction for more anisotropic particles.

5. Conclusion

Anisotropic particles in the shape of elliptical and rectangular prisms are fabricated to study their particle-field interactions with external AC electric field. It is found that the ellipsoidal theory works for elliptical prisms with a newly found consistent particle conductivity value while the adjustable multiplier for geometry factor is introduced to solve the bad agreement between ellipsoidal theory and experiment for rectangular prisms. Based on precedent work investigating the interaction for superellipsoid particles, new anisotropic particles are fabricated using photolithographic method, and we further observed and analyzed the translational and

orientational motion of newly made dielectric anisotropic particles in equilibrium electric field conditions. To reduce the difference between theory and experiments, a general conductivity value of 110 leads to excellent agreement in particle-field potentials for all tested particles is found. The generated 2D and 1D energy landscapes shows that a good agreement between theory and experiment can be found for elliptical prisms with various aspect ratios with a similar particle conductivity. The multiplier for geometry factor needs to be introduced to address the disagreement caused by geometric issue for rectangular prisms with sharp rounded corners. This modification is reasonable since the main difference between the two anisotropic particles is the sharp rounded corners that rectangular prism possesses. From the generated results and figures, some acceptable agreements between theory and experiments can be found, and a general conclusion can be obtained with the application of physical restriction showing that the multiplier for geometry factor in x and y direction are always smaller than 1 while the one in z direction is bigger than 1 with similar results for different rectangular prisms. In the future, more work should be done to reveal the meaning of multiplier for geometry factor and the derivation of dipole-field interaction for other anisotropic particles.

6. References

1. Liyu Wang, Y. Y., Yonghua Chen, Carmel Majidi, Fumiya Iida, Erin Askounis, and Qibing Pei, Controllable and reversible tuning of material rigidity for robot applications. *Mater. Today* **2018,** *21* (5).

2. Faezeh Arab Hassani, Q. S., Feng Wen, Tianyiyi He, Ahmed Haroun, Yanqin Yang, Yuqin Feng, and Chengkuo Lee, Smart materials for smart healthcare– moving from sensors and actuators to self-sustained nanoenergy nanosystems. *Smart Materials in Medicine* **2020,** *1*.

3. Minxuan Kuang , L. W., and Yanlin Song, Controllable Printing Droplets for High-Resolution Patterns. *Adv. Mater.* **2014,** *26*.

4. Sharon C. Glotzer, M. J. S., Anisotropy of building blocks and their assembly into complex structures. *Nat. Mater.* **2007,** *6*.

5. Fuduo Ma, X. Y., and Ning Wu, Directed assembly of anisotropic particles under external fields. In *Anisotropic Particle Assemblies*, Ning Wu, D. L., and Alberto Striolo, Ed. Elsevier: 2018.

6. A. Ashkin, J. M. D., J. E. Bjorkholm, and Steven Chu, Observation of a single-beam gradient force optical trap for dielectric particles. *Opt. Lett.* **1986,** *11* (5).

7. A. N. Grigorenko, N. W. R., M. R. Dickinson, and Y. Zhang, Nanometric optical tweezers based on nanostructured substrates. *Nat. Photonics* **2008,** *2*.

8. Angel Martinez, H. C. M., and Ivan I. Smalyukh, Large-area optoelastic manipulation of colloidal particles in liquid crystals using photoresponsive molecular surface monolayers. *Proc. Natl. Acad. Sci. U.S.A.* **2011,** *108* (52).

9. Jingang Li, Y. L., and Yuebing Zheng, Light-Directed Nanomanipulation of Colloidal Particles in Ambient Environments. *2019 Conference on Lasers and Electro-Optics (CLEO)* **2019**.

10. Peter John Rodrigo, V. R. D., and Jesper Glückstad, Four-dimensional optical manipulation of colloidal particles. *Appl. Phys. Lett* **2005,** *86*.

11. Ahmet F. Demirörs, P. P. P., Bartlomiej Kowalczyk, and Bartosz A. Grzybowski, Colloidal assembly directed by virtual magnetic moulds. *Nature* **2013,** *503*.

12. Alexey Snezhko, I. S. A., Magnetic manipulation of self-assembled colloidal asters. *Nat. Mater.* **2011,** *10*.

13. Benjamin B. Yellen, O. H., and Gary Friedman, Arranging matter by magnetic nanoparticle assemblers. *Proc. Natl. Acad. Sci. U.S.A.* **2005,** *102* (25).

14. Di Du, D. L., Madhuri Thakur, and Sibani Lisa Biswal, Generating an in situ tunable interaction potential for probing 2-D colloidal phase behavior. *Soft Matter* **2013,** *9*.

15. Mingsheng Wang, L. H., and Yadong Yin, Magnetic field guided colloidal assembly. *Mater. Today* **2013,** *16* (4).

16. N. Osterman, I. P., J. Dobnikar, D. Frenkel, P. Ziherl, and D. Babic, Field-Induced Self-Assembly of Suspended Colloidal Membranes. *Phys. Rev. Lett.* **2009,** *103*, 4.

17. Pietro Tierno, A. S., Tom H. Johansen, and Francesc Sagués, Dynamic colloidal sorting on a magnetic bubble lattice. *Appl. Phys. Lett.* **2008,** *93*.

18. Shuo Wang, Y. C., Xuemao Zhou, Lijie Lei, Zameer Hussain Shah, Guanhua Lin, and Yongxiang Gao, Magnetic Manipulation and Assembly of Nonmagnetic Colloidal Rods in a Ferrofluid. *Langmuir* **2021,** *37*.

19. A. van Blaaderen, M. D., R. van Roij, A. Imhof, M. Kamp, B. W. Kwaadgras, T. Vissers, and B. Liu, Manipulating the self assembly of colloids in electric field. *Eur. Phys. J.* **2013,** *222*.

20. David Pritchet , K. E., Jian Cao, and Jiaxing Huang, Manipulation and Localized Deposition of Particle Groups with Modulated Electric Fields. *Micromachines* **2020,** *11*, 28.

21. Jaime J. Juárez, M. A. B., Interactions and microstructures in electric field mediated colloidal assembly. *J. Chem. Phys.* **2009,** *131*.

22. Maruti Uppalapati, Y.-M. H., Thomas N. Jackson, and William O. Hancock, Microtubule Alignment and Manipulation Using AC Electrokinetics. *Small* **2008,** *4* (9).

23. Souvik Ghosh, A. G., All optical dynamic nanomanipulation with active colloidal tweezers. *Nat. Commun.* **2019,** *10*, 8.

24. Linhan Lin, E. H. H., Xiaolei Peng, and Yuebing Zheng, Optothermal Manipulations of Colloidal Particles and Living Cells. *Acc. Chem. Res.* **2018,** *51* (6).

25. Souvik Ghosh, A. G., Mobile nanotweezers for active colloidal manipulation. *Sci. Robot.* **2018,** *3* (14).

26. Randall A. Meyer, J. J. G., Shaping the Future of Nanomedicine: Anisotropy in Polymeric Nanoparticle Design. *Wiley Interdiscip. Rev. Nanomed. Nanobiotechnol.* **2016,** *8* (2).

27. Laura Rossi, S. S., William T. M. Irvine, Paul M. Chaikin, David J. Pine, and Albert P. Philipse, Cubic crystals from cubic colloids. *Soft Matter* **2011,** *7*.

28. Anke Kuijk, A. v. B., and Arnout Imhof, Synthesis of Monodisperse, Rodlike Silica Colloids with Tunable Aspect Ratio. *J. Am. Chem. Soc* **2011,** *133*.

29. Kyung Jin Lee, J. Y., and Joerg Lahann, Recent advances with anisotropic particles. *Curr. Opin. Colloid Interface Sci.* **2011,** *16*.

30. Lingling Ge, J. C., Duo Wei, Yue Sun, and Rong Guo, Anisotropic Particles Templated by Cerberus Emulsions. *Langmuir* **2018,** *34*.

31. Mona Tréguer-Delapierre, A. M., Céline Hubert, and Serge Ravaine, Recent advances in the synthesis of anisotropic particles. In *Anisotropic Particle Assemblies*, Ning Wu, D. L., and Alberto Striolo, Ed. Elsevier: 2018; p 35.

32. Orlin D. Velev, S. G., and Dimiter N. Petsev, Particle-localized AC and DC manipulation and electrokinetics. *Annu. Rep. Prog. Chem., Sect. C* **2009,** *105*.

33. Orlin D. Velev, K. H. B., On-chip micromanipulation and assembly of colloidal particles by electric fields. *Soft Matter* **2006,** *2*.

34. Bradley Rupp, I. T.-D., Xiaoqing Hua, and Michael A. Bevan, Measurement of Anisotropic Particle Interactions with Nonuniform ac Electric Fields. *Langmuir* **2018,** *34*.

35. Egor V. Yakovlev, K. A. K., Kirill I. Zaytsev, Nikita P. Kryuchkov, Kirill I. Koshelev, Arsen K. Zotov, Dmitry A. Shelestov, Victor L. Tolstoguzov, Vladimir N. Kurlov, Alexei V. Ivlev, and Stanislav O. Yurchenko, Tunable two-dimensional assembly of colloidal particles in rotating electric fields. *Sci. Rep.* **2017,** *7*, 10.

36. Sumit Gangwal, O. J. C., and Orlin D. Velev, Dielectrophoretic Assembly of Metallodielectric Janus Particles in AC Electric Fields. *Langmuir* **2008,** *24*.

37. Stratton, J. A., *Electromagnetic Theory*. McGraw-Hill Book Company, Inc: New York, 1941.

38. O'Konski, C. T., Electric Properties of Macromolecules. V. Theory of Ionic Polarization in Polyelectrolytes. *J. Phys. Chem.* **1960,** *64* (5), 605.

39. Hywel Morgan, A. G. I., David Bakewell, Nicolas G Green, and Antonio Ramos, The dielectrophoretic and travelling wave forces generated by interdigitated electrode arrays: analytical solution using Fourier series. *J. Phys. D: Appl. Phys.* **2001,** *34*.

40. Lide, D. R., *CRC Handbook of Chemistry and Physics*. CRC Press: New York, 2000.

41. Jaime J. Juarez, J.-Q. C., Brian G. Liu, and Michael A. Bevan, kT-Scale Colloidal Interactions in High Frequency Inhomogeneous AC Electric Fields. I. Single Particles. *Langmuir* **2011,** *27*.

42. Julie L. Bitter, Y. Y., Gregg Duncan, Howard Fairbrother, and Michael A. Bevan, Interfacial and Confined Colloidal Rod Diffusion. *Langmuir* **2017,** *33*.

43. L. A. Apresyan, D. V. V., On Depolarization Factors of Anisotropic Ellipsoids in an Anisotropic Medium. *Tech. Phys.* **2014,** *59* (12).

44. Sihvola, A., Metamaterials and Depolarization Factors. *Prog. Electromagn. Res.* **2005,** *51*.